Domain Motions of the Mip Protein from *Legionella pneumophila*[†,‡]

Martin Horstmann,[§] Philipp Ehses,[§] Kristian Schweimer,[||] Michael Steinert,[⊥] Thilo Kamphausen,[@,+] Gunter Fischer,[@] Jörg Hacker,[⊥] Paul Rösch,[||] and Cornelius Faber*[,§]

Lehrstuhl für Experimentelle Physik 5, Universität Würzburg, Würzburg, Germany, Lehrstuhl für Biopolymere, Universität Bayreuth, Bayreuth, Germany, Max-Planck-Forschungsstelle für Enzymologie der Proteinfaltung, Halle, Germany, and Institut für Molekulare Infektionsbiologie, Universität Würzburg, Würzburg, Germany

Received April 26, 2006; Revised Manuscript Received August 15, 2006

ABSTRACT: The homodimeric 45.6 kDa (total mass) Mip protein, a virulence factor from *Legionella pneumophila*, was investigated with solution NMR spectroscopy and molecular dynamics (MD) simulations. Two Mip monomers are dimerized via an N-terminal helix bundle that is connected via a long α-helix to a C-terminal FKBP domain in each subunit. More than 85% of the amino acids were identified in triple-resonance NMR spectra. ^{15}N relaxation analysis showed a bimodal distribution of R_1/R_2 values, with the lower ratio in the N-terminal domain. Relaxation dispersion measurements confirmed that these reduced ratios did not originate from conformational exchange. Thus, two different correlation times (τ_c) can be deduced, reflecting partly uncoupled motions of both domains. Relaxation data of a Mip$^{77-213}$ monomer mutant were similar to those observed in the dimer, corroborating that the FKBP domain, including part of the connecting helix, behaves as one dynamic entity. MD simulations (18 ns) of the Mip dimer also yielded two different correlation times for the two domains and thus confirm the independence of the domain motions. Principal component analysis of the dihedral space covariance matrix calculated from the MD trajectory suggests a flexible region in the long connecting helix that acts as a hinge between the two domains. Such motion provides a possible explanation of how Mip can bind to complex molecular components of the extracellular matrix and mediate alveolar damage and bacterial spread in the lung.

The macrophage infectivity potentiator (Mip)[1] protein is one of the major virulence factors of Legionnaires' disease bacterium *Legionella pneumophila.* Similar proteins are expressed in all species of the genus *Legionella.* Mip belongs to the enzyme family of FK506 binding proteins (FKBP) and exhibits peptidyl prolyl *cis*/*trans* isomerase activity (PPIase, EC 5.2.1.8). It plays an important role in the intracellular infection of phagocytic host cells such as human alveolar macrophages and a number of freshwater protozoa (*1*). In guinea pig animal models, Mip potentiates infection (*2*). There, it was shown that both the PPIase activity and the full-length structure of the Mip dimer are crucial for full virulence of *Legionella* (*3*). More recently, Mip was demonstrated to contribute to bacterial dissemination within lung tissue after intratracheal infection of guinea pigs. Transwell assays revealed that only Mip-positive *Legionella* bacteria transmigrate across an in vitro lung epithelium barrier of NCI-H292 lung epithelial cells and extracellular matrix. By using binding assays, Mip has been shown to bind specifically to the extracellular matrix component collagen IV (*4*). However, the exact interaction of Mip and collagen has not been elucidated.

Mip is a basic 2 × 22.8 kDa surface protein (pI 9.8) forming homodimers present in both solution and on the outer membrane of *L. pneumophila*, as has been demonstrated by cross-linking experiments (*5*, *6*). The crystal structure of Mip (Figure 1) revealed that each monomer consists of an N-terminal dimerization module connected via a long (6.5 nm) α-helix to the C-terminal peptidyl prolyl *cis*/*trans* isomerase (PPIase) domain. The homodimerization of Mip is mediated by an unusual four-helix bundle, involving two helices from the N-terminal domain of each monomer (*7*). The fold of the C-terminal domain (residues G100−S213) resembles the human FK506-binding protein (FKBP12). This domain is also responsible for the binding of the immunosuppressants FK506 and rapamycin, which efficiently inhibit PPIase activity (*8*). In proteins with a similar overall topology, such as calmodulin or troponin C, apparently rigid connecting α-helices have been shown,

[†] This work was funded by the German Research Foundation (SFB 630, projects C2 and B1).

[‡] NMR chemical shifts and relaxation data are available via BMRB entry 7021.

* To whom correspondence should be addressed: Lehrstuhl für Experimentelle Physik 5, Universität Würzburg, Am Hubland, 97070 Würzburg, Germany. Telephone: (49) 931 888 5110. Fax: (49) 931 888 5851. E-mail: faber@physik.uni-wuerzburg.de.

[§] Lehrstuhl für Experimentelle Physik 5, Universität Würzburg.

[||] Universität Bayreuth.

[⊥] Institut für Molekulare Infektionsbiologie, Universität Würzburg.

[@] Max-Planck-Forschungsstelle für Enzymologie der Proteinfaltung.

[+] Present address: Strathmann Biotec GmbH & Co. KG, Biotechnologiezentrum, Dengelsberg, 24796 Bovenau, Germany.

[1] Abbreviations: CPMG, Carr−Purcell−Meiboom−Gill; PCA, principle component analysis; ED, essential dynamics; MD, molecular dynamics; dPCA, principle component analysis in dihedral space; TROSY, transverse relaxation optimized spectroscopy; NMR, nuclear magnetic resonance; CSI, chemical shift index; NOE, nuclear Overhauser effect; NOESY, nuclear Overhauser spectroscopy; BMRB, Biological Magnetic Resonance Data Bank; FKBP, FK506 binding protein; Mip, macrophage infectivity potentiator; PPIase, peptidyl prolyl *cis*/*trans* isomerase activity; LINCS, linear constraint solver; SPC, single-point charge; HSQC, heteronuclear single-quantum coherence; PME, particle mesh ewald.

10.1021/bi060818i CCC: $33.50 © 2006 American Chemical Society
Published on Web 09/16/2006

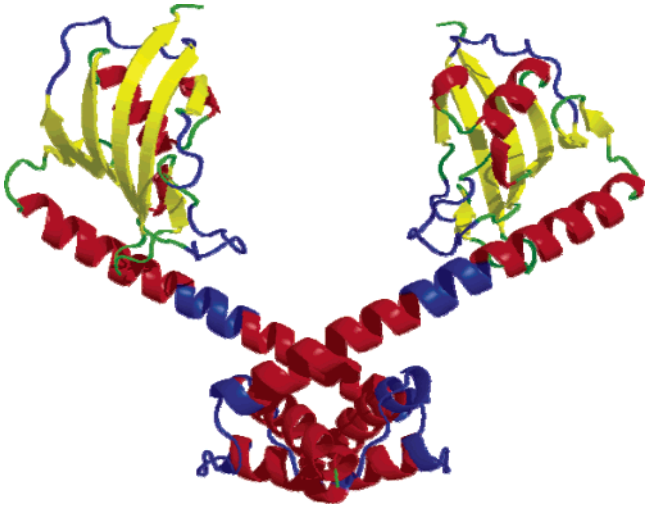

FIGURE 1: Schematic representation of the crystal structure of the Mip dimer (*7*). The N-terminal dimerization domain is connected to the C-terminal FKBP domains by a long α-helix. The monomer mutant Mip$^{77-213}$ comprises the second half of the long α-helix and the FKBP domain. The color blue marks flexible regions as identified by dPCA of the MD trajectory (see the text and Figure 9).

however, to be flexible. Large interdomain motions were observed, which are crucial for molecular recognition processes (*9*, *10*). NMR spectroscopy affords versatile tools for identifying and characterizing such domain motions (*11*, *12*). Analysis of nuclear spin relaxation gives information about local dynamics as well as domain motions. In conjunction with molecular dynamics (MD) simulations, interdomain motions and hinges connecting domains can be identified (*13*). Here, we use a combined NMR−MD approach to identify domain motions of the Mip protein.

EXPERIMENTAL PROCEDURES

NMR Experiments. Escherichia coli harboring a plasmid encoding Mip were used to overproduce Mip in ^{13}C-, ^{15}N-, and 50% D-labeled medium (Spectra 9, Spectra Gases, Inc., Branchburg, NJ). Mip was purified from these bacteria as described previously (*3*). The sample used for NMR experiments contained 0.9 mM triply labeled (50% D, 98% ^{13}C, 98% ^{15}N) Mip dissolved in 20 mM potassium phosphate buffer in 90% H_2O and 10% D_2O (pH 6.5). For experiments with the Mip$^{77-213}$ monomer mutant lacking the dimerization domain but containing the PPIase domain, a 2.5 mM sample of doubly labeled (98% ^{13}C, 98% ^{15}N) Mip$^{77-213}$ was produced as described previously (*14*).

All NMR experiments were performed on Bruker Avance 600, 700, or 800 MHz spectrometers at 298 K. The data were processed using NMRPipe (*15*).

Sequence-specific backbone assignments were obtained from TROSY (*16*) versions of three-dimensional HNCO, HNCA, HNCACB, and HN(CO)CACB experiments. For the assignment of side chain resonances, HBHA(CO)NH, CCONH, and HCCH-TOCSY spectra were recorded.

Backbone and side chain assignments was supported by connectivities from ^{15}N NOESY, ^{13}C NOESY, and ^{15}N−^{15}N NOESY spectra (mixing time of 120 ms).

Peak picking and visualization of the spectra were performed using NMRview (*17*). The secondary structure was predicted by consensus ($^{1}H_{\alpha}$, $^{13}C_{\alpha}$, ^{13}CO) chemical shift indexing (*18*, *19*).

The ^{1}H−^{15}N relaxation experiments were performed at 600 MHz using pulse sequences of Dayie and Wagner (*20*, *21*). The R_1 values were determined by recording 11 experiments with eight different delays [5.38 (two times), 32.20, 64.38, 128.73 (two times), 300.35, 697.21 (two times), 1297.87, and 1995.06 ms]. To determine the R_2 values, 11 experiments with five different delays [16.96 (two times), 50.84 (two times), 101.65 (three times), 152.47 (two times), and 203.28 ms (two times)] were performed. For the measurement of the heteronuclear ^{1}H−^{15}N NOE, the relaxation delay was set to 4 s. Proton saturation was achieved with 600 high-power pulses with an interpulse delay of 5 ms for the final 3 s of the relaxation delay in the saturation experiment.

Dispersion of R_2 relaxation rates as a function of ν_{CPMG}, the CPMG pulse repetition frequency, was examined by experiments described by Kay et al. (*22*, *23*). The intensities of cross-peaks in two-dimensional ^{1}H−^{15}N HSQC spectra recorded for a given ν_{CPMG} were converted into decay rates

$$R_2(\nu_{CPMG}) = \frac{-1}{T} \ln \frac{I(\nu_{CPMG})}{I_0} \qquad (1)$$

where $I(\nu_{CPMG})$ and I_0 are the intensities of a given cross-peak with and without the CPMG periods, respectively, and $\nu_{CPMG} = 1/(4\tau_{CPMG})$, with $2\tau_{CPMG}$ being the separation between the centers of successive refocusing pulses. $R_2(\nu_{CPMG})$ values were recorded three times for ν_{CPMG} values of 50 (three times), 100 (three times), 200 (three times), and 500 (three times) Hz with an overall echo time of 80 ms, as well as three times without the CPMG period for 0 ms (three times).

Correlation times (τ_c) averaged over different regions of the protein were calculated using the TENSOR2 software package (*24*, *25*) assuming isotropic tumbling. Only relaxation rates of residues showing an HetNOE of >0.65 were used.

MD Simulations. MD calculations were performed on a quad Opteron 850 (2.4 GHz) HP ProLiant server (Debian Linux with 16 GB Ram) using Gromacs 3.3 (*26*−*28*). For the MD simulation, the crystal structure of the Mip dimer composed of two symmetric monomer subunits (residues T9−S212, PDB entry 1FD9) was used as the starting structure (*7*). The protein was solvated in a periodic box with 11 859 SPC water molecules (*29*). Electrostatic interactions were calculated by the fast particle mesh Ewald (PME) algorithm with a cutoff of 0.9 nm (*30*). The temperature was controlled by Berendsen temperature coupling, a weak coupling to a bath with a constant temperature (*31*). The chemical bond lengths and dihedrals were constrained after each time step of 2 fs by the LINCS algorithm (*32*). All simulations were conducted using the GROMACS force field (*26*−*28*, *33*).

The initial part of the simulation followed a nonrestraint protocol where the energy of the system was minimized until the energy converged and all close contacts were removed from the system. Subsequently, the water molecules were allowed to equilibrate for 40 ps around the fixed protein to fill holes which were not populated by the SPC water box. Finally, an 18 ns MD run was executed with the energy-minimized and solvated protein.

The principal component analysis (PCA), also termed essential dynamics (ED), of MD trajectories is tailored specifically for interdomain motion analysis where large anharmonic fluctuations occur (*34*). Especially, the PCA in dihedral space (dPCA) of backbone torsion angles (Φ and Ψ) is a valuable tool for revealing hinges or hinge regions between domains (*34*−*36*).

The covariance matrix **C** is normally calculated for atomic coordinates.

$$C_{ij} = \frac{1}{S}\sum[x_i(t) - \langle x_i\rangle][x_j(t) - \langle x_j\rangle] \quad (2)$$

where S is the total number of configurations ($t = 1, 2, 3, ..., N$), $x_i(t)$ values are the position coordinates, where $i = 1, 2, ..., 3N$, and N is the number of atoms for which **C** is calculated. For the heavy atoms of the protein backbone (N, C_α, C, and O), this results in 12 degrees of freedom per amino acid. The real degrees of freedom for a protein backbone are more likely the rotations around the N−C_α (Φ) and C_α−C (Ψ) bonds which were extracted with Gromacs "*rama*" tool. Therefore, we have diagonalized the covariance matrix **C** for 203 backbone angle pairs (Φ and Ψ) of each monomer subunit of Mip using a self-written python program. This dPCA yielded two sets of 203 pairs of eigenvalues and corresponding eigenvectors.

The theory of correlation functions is well-established, and for comparison with NMR rotational correlation times (τ_c), the rotational autocorrelation function (ACF) $G_r(\tau)$ for any N−H vector of the backbone can be calculated by (*37*)

$$G_r(\tau) = \langle P_n[\mu(t)\mu(0)]\rangle$$

$$G_r(\tau) = \sum_{i=1}^{N}\langle P_n[\mu(\tau_i)\mu(t+\tau_i)]\rangle \quad (3)$$

where N is the number of time steps used for the calculation, $\mu(t)$ is the N−H vector at time t, and P_n is the nth Legendre-Polynom ($n = 2$). The ACF is usually modeled by an exponential decay:

$$G_r(\tau) = e^{-t/\tau} \quad (4)$$

The correlation time τ can be calculated by fitting eq 4 to the ACF obtained from the trajectory of a MD simulation according to eq 3. To compare the results with NMR data, we have calculated τ separately for one whole monomer unit of Mip, the FKBP domain, and the dimerization domain.

RESULTS

Resonance Assignment. A prerequisite for analysis of NMR data was the assignment of resonance lines. At 45.6 kDa, the Mip dimer has to be considered large for NMR experiments. For the rigid crystal structure, a rotational correlation time of 45.8 ns was calculated with HYDRONMR (*38*). Consequently, deuteration and application of TROSY were mandatory. Partial (50%) deuteration was sufficient for obtaining high-resolution NMR data, hinting that internal motions in Mip may shorten the effective correlation time for relaxation. In triple-resonance and NOESY NMR spectra, most backbone resonances of Mip were identified (Figure 2). Overall, ~86% of HN, C_α, and C_β, 79% of CO, and 74% of H_α resonances were assigned. The H_β side chain resonance assignment was completed to >69%. The other side chain resonances were only partly

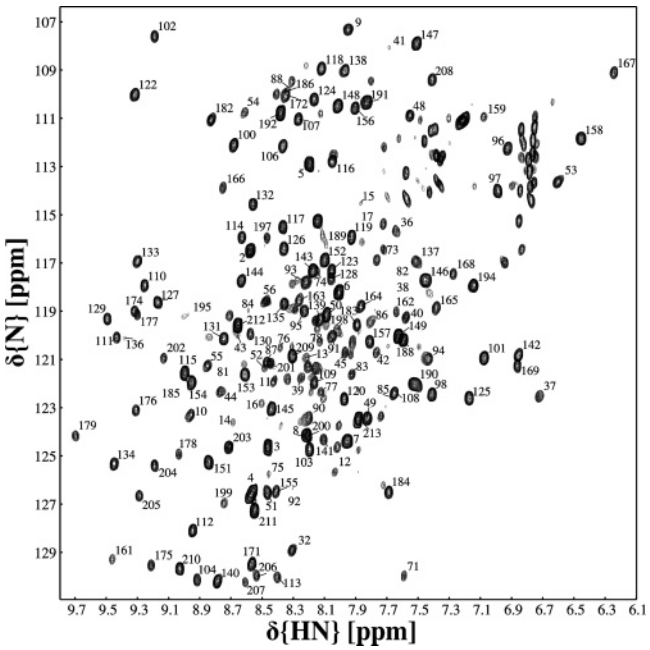

FIGURE 2: Assignment of Mip shown in a three-dimensional HNCO spectrum projected onto the $^1H-^{15}N$ plane. The numbering is according to residues in the protein.

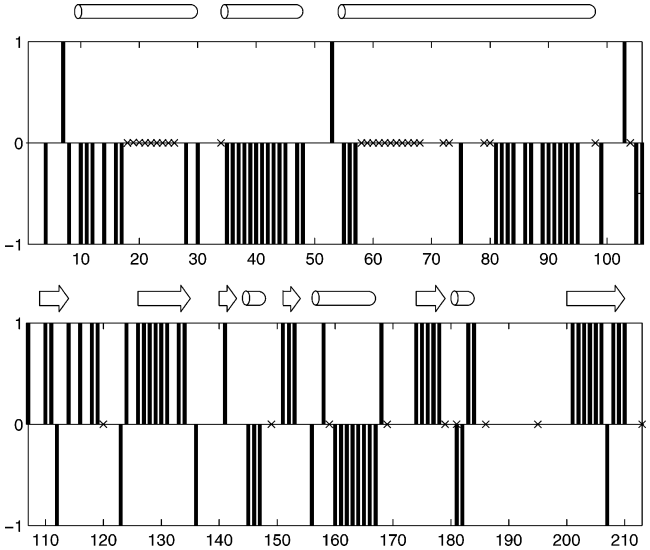

FIGURE 3: Consensus (H_α, C_α, and C′) CSI compared with secondary structure elements derived from the crystal structure of Mip (PDB entry 1FD9). All elements are conserved in solution. Amino acids that were not assigned (at least two of the three consensus shifts) are denoted as X.

Table 1: Unambiguously Assigned Intermolecular NOEs in Homodimeric Mip

	chemical shift (ppm)			chemical shift (ppm)		distance in the crystal structure (Å)
	H	C		H	C	
12 H_α	4.22	58.36	37 H_β	1.41	18.43	3.54
12 H_β	2.6	40.05	37 H_β	1.41	18.43	4.01
15 $H_{\beta1}$	3.98	63.93	38 H_β	1.64	31.9	2.33
15 $H_{\beta1}$	3.98	63.93	38 HN	7.65	118.3	3.33
16 H_β	2.87	18.43	37 H_β	1.41	39.74	2.8
16 HN	8.49	122.53	37 H_β	1.41	18.43	2.95

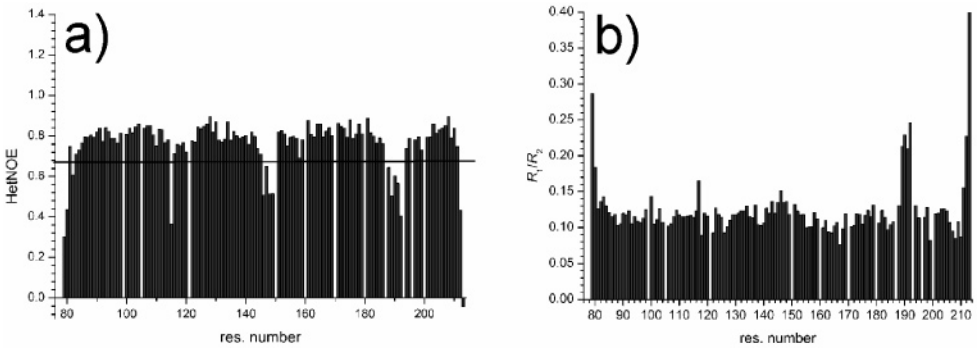

FIGURE 4: Relaxation data of Mip$^{77-213}$ measured at 14.1 T. (a) ^{1}H−^{15}N HetNOE values for each residue. Values below the threshold of 0.65 (bold black line) are indicative of motion on a fast picosecond time scale (*39*). (b) R_1/R_2 values for each residue.

identified. In the C-terminal half (from residue A81), more than 97% of the backbone resonances (heavy atoms) and ~85% of H_α and H_β signals were assigned. All chemical shifts were similar to those found in the Mip$^{77-213}$ monomer mutant (*14*). Residues that were not found in the spectra were mainly from two contiguous stretches in the N-terminal half of the protein. Signal intensity continuously decreased when proceeding along the backbone from very strong signals of the N-terminal residues to I18. Resonances for residues G19−F26, forming roughly the second half of the N-terminal helix, could not be found in the spectra. Similarly, residues M58−K69, forming roughly the first half of the long connecting helix, were not identified. Chemical shift data and heteronuclear relaxation data were deposited in the Biological Magnetic Resonance Bank, as entry 7021.

The chemical shift index (CSI) indicates that the secondary structure elements observed in the crystal structure are also present in solution in full-length Mip (Figure 3) and Mip$^{77-213}$ (data not shown). Close contacts between the C-terminal part of the connecting helix (residues G80−K98) and the FKBP domain are confirmed by nuclear Overhauser effect (NOE) signals observed in both the dimer and the monomer mutant Mip$^{77-213}$. The existence of the Mip dimer in solution is confirmed by several NOEs in three-dimensional NOESY-HSQC spectra. Between the two monomer subunits, six interactions were identified unambiguously at each ^{13}C or ^{15}N frequency corresponding to the heavy atom where the interacting hydrogen is attached (Table 1).

Relaxation Analysis. Relaxation rates R_1 and R_2 and the heteronuclear NOE (HetNOE) of the ^{15}N amide in the backbone were measured and analyzed for both full-length Mip and monomeric Mip$^{77-213}$. HetNOE values and relaxation rates confirm the presence of a stable secondary structure as observed in the crystal structure of both the dimer and the monomer. In Mip$^{77-213}$, HetNOE values of <0.65 were observed at both termini, indicating fast motion on a picosecond time scale typical for unstructured highly flexible termini (*39*) (Figure 4a). Similarly, HetNOE values suggest fast motion for residues R188−G192 and K146−K149, both regions in flexible loops in the crystal structure. The R_1/R_2 values are also elevated at both termini and for the stretch of S189−G192 (Figure 4b). For full-length Mip, analysis was possible for 156 residues despite some signal overlap and partially low intensity. Only for two contiguous stretches, residues I18−P35 and residues Q57−K69, could no data be obtained. HetNOE values of <0.65 were observed for terminal residues T2−L7, S212, and S213, for residues

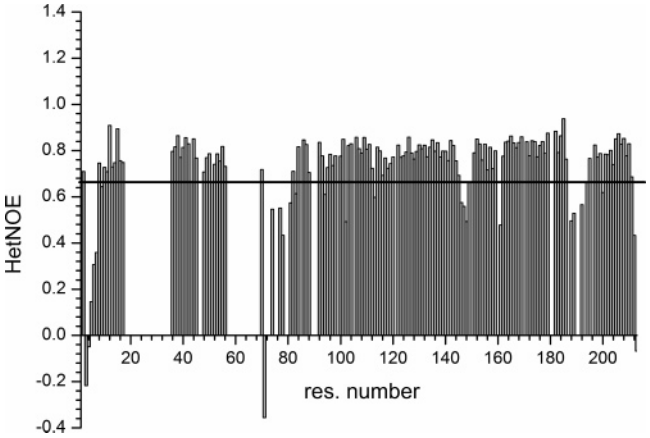

FIGURE 5: ^{1}H−^{15}N HetNOE of full-length Mip measured at 14.1 T. Values below the threshold of 0.65 (bold black line) are indicative of motion on a fast picosecond time scale (*39*).

R188−G192 and K146−G148, and additionally for the region between residues M70 and K80 in the long connecting helix (Figure 5).

The ratio of longitudinal to transverse relaxation rates (R_1/R_2) scales inversely with the rotational correlation time (τ_c) and thus is indicative of domain motion (*11*). For full-length Mip, increased values were observed for the regions suggested to be flexible by the HetNOE data (Figure 6a). A histogram of R_1/R_2 over all residues (Figure 6b) reveals a bimodal distribution of the values. Two Gaussian distributions fitted to the histogram yielded maxima at 0.081 ± 0.01 and 0.13 ± 0.01, suggesting that the two distributions can be clustered for the dimerization domain (for residues A8−Q56, $R_1/R_2 = 0.081$) and the FKBP domain, including part of the connecting α-helix ($R_1/R_2 = 0.13$) (Figure 6a). Exact definition of the residues contributing to each of the distributions cannot be determined from the histogram.

The different R_1/R_2 values in the dimerization domain and the C-terminal part of Mip can have two possible origins. First, partly independent motion of each domain can lead to different correlation times (τ_c) reflected in different R_1/R_2 values. Second, conformational exchange on a millisecond time scale may contribute to transverse relaxation and lead to overestimation of R_2 (*40*, *41*). This second possible origin was investigated with relaxation dispersion measurements which allow identification of exchange contributions to R_2. For full-length Mip, relaxation dispersion curves, $R_2(\nu_{CPMG})$, were obtained for 144 residues. Except for residues M42 and G186, no significant dispersion was observed (Figure 7). These data clearly demonstrate that contributions to R_2

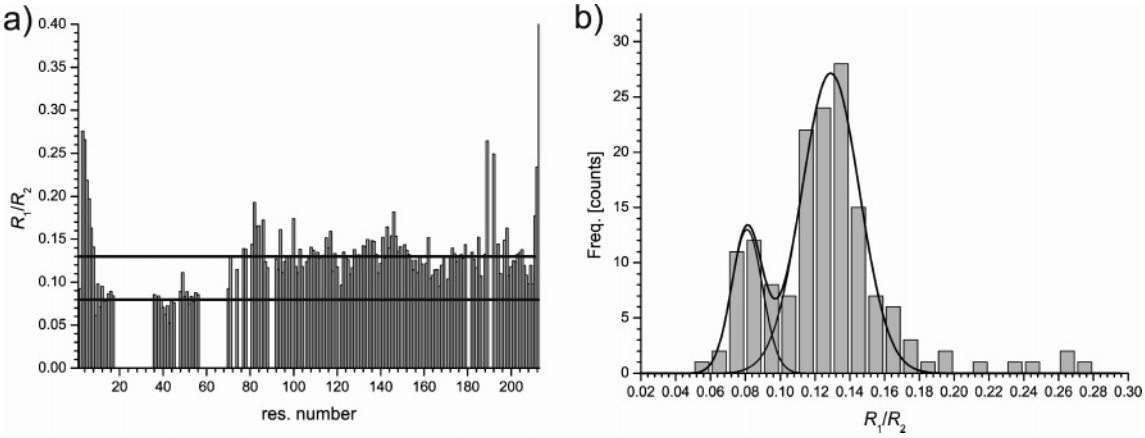

FIGURE 6: (a) R_1/R_2 measured at 14.1 T. Bold black lines at $R_1/R_2 = 0.08$ and $R_1/R_2 = 0.13$ indicate the maxima of the two Gaussian distributions obtained from the histogram shown in panel b. The distribution clustered around 0.08 originates from residues A8−Q56 in the dimerization domain. The second distribution clustered around 0.13 pools residues from the C-terminal part of Mip. (b) Histogram of R_1/R_2 values. A bimodal distribution indicates that Mip consists of two domains with partly uncoupled motions.

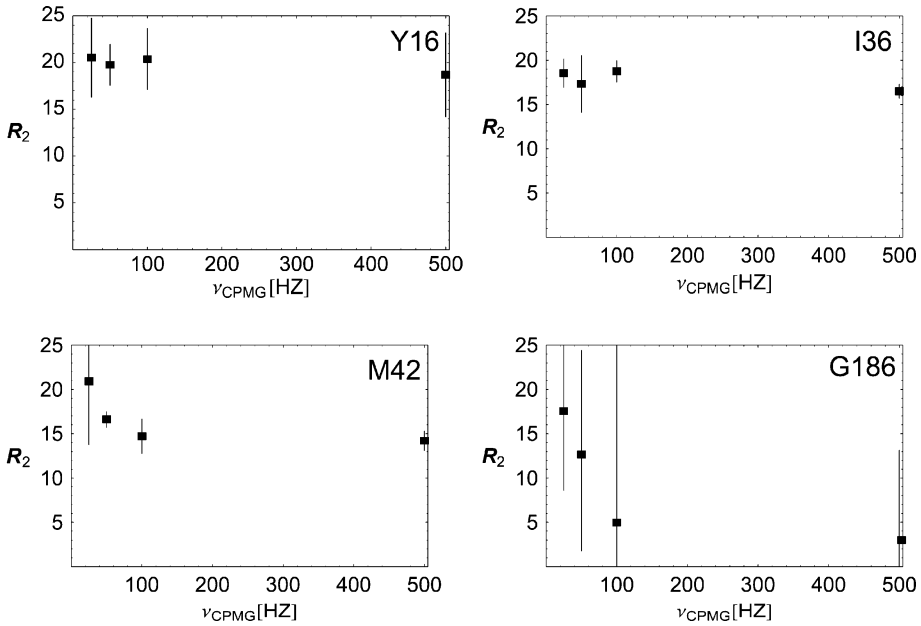

FIGURE 7: R_2 is plotted as a function of ν_{CPMG}. For the dimerization domain, curves for two exemplary residues (Y16 and I36) are displayed showing no dispersion (top row). Only for residues G186 and M42 is dispersion observed, indicating slow conformational exchange (bottom row).

from conformational exchange processes occur only for single residues. The lower R_2 values in the dimerization domain, as compared to the FKBP domain, do not result from millisecond motion but are rather indicative of slower overall tumbling. However, the possibility that dynamics on an intermediate time scale, which may play a role in formation and stabilization of the dimer, also influence the R_2 values cannot be totally ruled out.

To estimate the degree of decoupling of domain motions, overall correlation times for molecular tumbling were derived from the R_1/R_2 values. This derivation implies that the molecule tumbles isotropically without significant contributions from local motions. For Mip$^{77-213}$, a τ_c of 8.3 ns was obtained. When using only residues in the FKBP domain (G100−S213), τ_c was calculated to be 8.2 ns, indicating that the helix is rigidly attached to the FKBP domain in the monomer mutant. For full-length Mip, the same analysis, assuming a single correlation time for the whole protein, yielded a τ_c of 8.4 ns (Table 2), which is too short for a rigid, homodimeric protein with a total molecular mass of 45.6 kDa. The calculated value of the correlation time shows that the assumption of a rigid molecule is not valid and confirms the existence of partly uncoupled domain motions. When using only residues of the dimerization domain, the calculation yields a τ_c of 10.9 ns; when using only residues K80−S213, $\tau_c = 8.5$ ns, and $\tau_c = 8.3$ ns for residues G100−S213 (Table 2). The value obtained for the C-terminal part of Mip is nearly identical to the value obtained for the monomer mutant, suggesting that the FKBP domain performs motions that are nearly unrestricted by the rest of the protein. However, the possibility that partly coupled domain motions

Table 2: Rotational Correlation Times (τ_c) Obtained from NMR Relaxation Rates R_1 and R_2 and from MD/ACF Calculation

	Mip dimer	Mip dimer dimerization domain	Mip dimer residues K80−S213 (G100−S213)	Mip$^{77-213}$ (G100−S213)
NMR	8.4 ns	10.9 ns	8.5 ns (8.3 ns)	8.3 ns (8.2 ns)
MD/ACF	7.6 ns	10.3 ns	6.3 ns	−

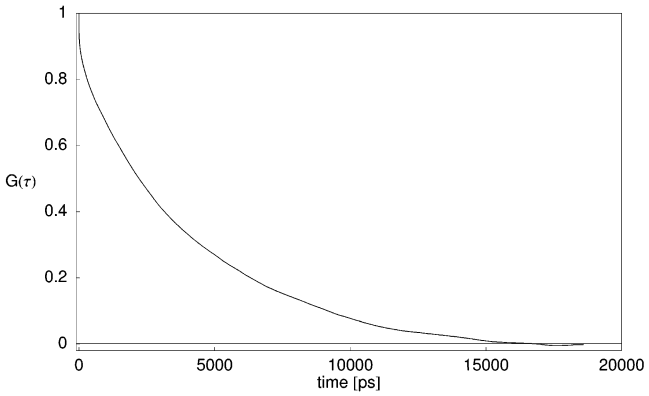

FIGURE 8: Autocorrelation function $G(\tau)$, as defined by eq 3 and averaged over all residues in the Mip dimer, calculated from the trajectory of the 18 ns MD simulation. The function levels off, indicating that the MD was long enough to describe the dynamics of the protein.

influence the calculated values cannot be ruled out, calling for an alternative investigation of the dynamics.

MD Analysis. To obtain more information about the domain motions that could not be derived from the NMR data, an 18 ns MD simulation of the Mip dimer solvated in water was performed. From the trajectory, ACFs for the N−H vectors were calculated according to eq 3. The ACF averaged over all N−H vectors in the dimer decays exponentially and levels off toward the end of the simulation (Figure 8), showing that the trajectory properly samples the dynamics of the protein. The rotational correlation times (τ_c) were calculated from the trajectory according to eqs 3 and 4. A τ_c of 7.6 ns was obtained for the whole dimer, and τ_c values of 10.6 and 6.3 ns were obtained for the dimerization domain and the extended FKBP domain (residues K80−S212), respectively. These values are in excellent agreement with the experimental data (Table 2) and confirm the independence of domain motions. The calculated τ_c value for the extended FKBP domain is slightly smaller than the experimental value obtained for the dimer and for Mip^{77-213}. This deviation possibly hints to an overestimation of overall motion by the MD simulation but confirms that the dynamics of the extended FKBP domain are partly decoupled from the rest of the dimer.

More detailed insight into the domain motions can be gained from analysis of the covariance matrix of the trajectory. The eigenvectors calculated in dihedral space describe anharmonic collective motions of the backbone rotations around Φ (N−C_α bond) and Ψ (C_α−C bond); 85% of the motions are represented by the first 10 eigenvector pairs (Figure 9). The strongest motions were observed in regions without defined secondary structure (see Figure 1) and also in the middle of the long connecting α-helix (black box in Figure 9). The flexible region in the helix was confined to ∼10 residues around N78, suggesting the existence of a hinge between the two domains. During the MD simulation, the helices in both subunits were strongly kinked in the hinge regions, allowing both FKBP domains to perform independent motions (Figure 10a). An overlay of extreme structures from MD simulations showed that the gap between the two FKBP domains increased from its original value of 3 nm to up to 6 nm during the simulation. Figure 10b schematically illustrates this opening of the dimer scaffold.

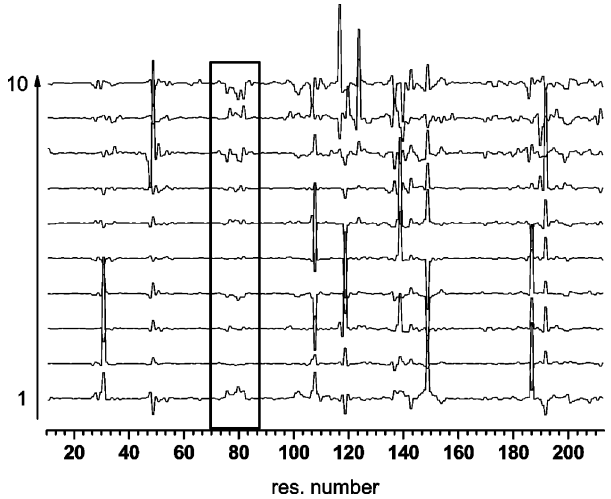

FIGURE 9: PCA in dihedral space (dPCA) of the trajectory of an 18 ns MD simulation of Mip in water. The first 10 eigenvectors in dihedral (Φ and Ψ) space are shown for one of the two monomer subunits. Anharmonic motions were observed only for regions without defined secondary structure and in the middle of the long connecting α-helix (black box). See also Figure 1.

DISCUSSION

NMR data yielded threefold evidence that the motions of the two domains are partly uncoupled. First, R_1/R_2 values show a domain-specific bimodal distribution. Second, relaxation data measured for Mip^{77-213} are very similar to those measured for the corresponding residues in the dimer, suggesting that motions of this part of Mip are dominated by the same dynamics in both molecules. Third, the τ_c obtained for the FKBP domain is significantly shorter than the τ_c for the dimerization domain, although molecular masses and the hydrodynamic radii are similar (in the dimer). Motion of the dimerization domain is dominated by the slower overall tumbling of the dimer, while the FKBP domains are free to move around the hinge in the connecting helix. However, our data do not allow for a detailed analysis of local dynamics and the exact degree of residual coupling between domain motions. Therefore, we have performed MD simulations to obtain more information about motions of the FKBP domains. Investigation of dynamics of the dimerization domain requires further experimental data and analysis taking into account local dynamics and couplings between the domains (*42*−*44*).

A prerequisite for a valid comparison between NMR relaxation data and MD simulations is that the crystal structure used as a template for MD correctly reflects the solution structure. NMR CSI indicated that the secondary structure elements in both full-length Mip and Mip^{77-213} are conserved with respect to the crystal structure. This is supported by the HetNOE values indicating flexible regions in the FKBP domain only in two loops in the crystal structure. Conservation of the fold of the dimerization domain is further corroborated by observation of intermonomer NOEs (Table 1). Without stabilization by the other monomer, tertiary structure is likely to be unstable in the helix bundle. Furthermore, the relaxation data for the residues of the N-terminal domain clearly indicate dimerization. Uncomplexed, the N-terminal α-helix bundle would open and display higher mobility, resulting in a shorter rotational correlation time (τ_c). Our experimental relaxation data show

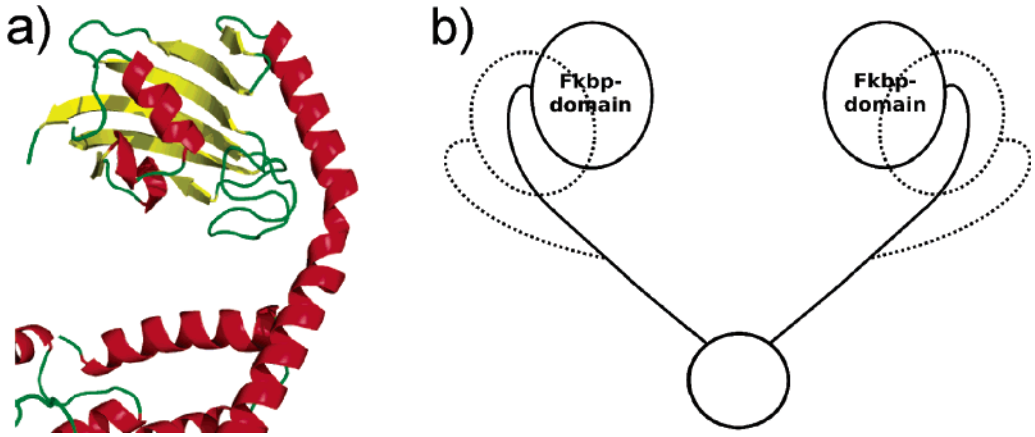

FIGURE 10: Hinge in the connecting α-helix that partly decouples domain motions. (a) A snapshot from the 18 ns MD simulation of Mip in water, showing one representative monomer subunit. The long α-helix connecting FKBP and the dimerization domain is kinked in the hinge region. (b) Schematic illustration of the effect of the hinge in the connecting α-helix. The distance between the two FKBP domains varies over time, allowing Mip to bind to target molecules larger than those that can bind with a rigid structure.

the opposite. Independent proof of Mip as a dimer in solution has previously been provided by cross-linking experiments (*5*, *6*). Summarizing all evidence, we conclude that the fold of the two domains in solution is identical to the crystal structure and its use as a template for MD simulations is justified.

The MD simulation of the Mip dimer in water predicted uncoupled domain motions in a manner independent of NMR. The calculated rotational correlation times (τ_c) for the whole dimer, as well as for the two domains separately, agree well with those obtained by NMR (Table 2). This demonstrates that the simulations are appropriate for analysis of dynamics of Mip in solution and confirms previous results that showed that GROMACS provides robust and meaningful results, especially when compared to data derived from NMR (*33*). For identification of hinges, dPCA is particularly useful because in Cartesian PCA, large domain displacements may obscure concerted changes of dihedral angle that are typical for hinge motions (*36*). dPCA of the MD trajectory revealed strong collective torsion angle fluctuations in the middle of the long α-helix (residues T74−E83), where the secondary structure was not stable and the helix opened, allowing this region to act as a hinge and thus to decouple the motions of the two domains. In addition to the overall tumbling of the dimer, both FKBP domains were free to wobble around the hinge, leading to correlation times shorter than those expected for a rigid dimer.

Similar instabilities of helical secondary structures have been observed in other proteins. For calmodulin, which is also made up of two globular domains connected by an α-helix, bimodal domain motions were observed by both MD simulations and NMR experiments (*9*, *45*, *46*). The helix was found to be less stable than the crystal structure suggested (*46*), and opening of the helix was observed during MD simulation. Similarly for FkpA, the Mip homologue from *E. coli*, ^{15}N relaxation data revealed interdomain motions and opening of the connecting helix (*47*), while the crystal structure alleges a rigid orientation of the domains (*48*).

We conclude that the hinge in the helix allows for diffusion-driven wobbling motions of the FKBP domains, which leads to fluctuations of the distance between the two FKBP domains in a dimer, enabling Mip to act like a clip and bind to larger target molecules than would be possible with a rigid structure. This molecular flexibility might be relevant during the binding of the extracellular matrix component collagen IV. It has been hypothesized that Mip binds collagen via its C-terminal domain since active site-directed drugs rapamycin and FK506 efficiently inhibited the interaction. In addition, in vitro studies with an artificial lung epithelium barrier suggest that the Mip−collagen interaction promotes the alveolar septum transmigration of *Legionella*, which appears to be decisive during bacterial dissemination in lung tissue (*4*).

In summary, we have identified independent motions of the dimerization and FKBP domains of Mip. The combination of NMR relaxation analysis and MD simulations using the crystal structure as a template has proven to be a powerful strategy for analyzing the dynamics of Mip. dPCA of a MD simulation trajectory has revealed a molecular hinge mediating interdomain motions, which were reflected in relaxation rates measured by NMR.

ACKNOWLEDGMENT

We thank Prof. Jochen Balbach for stimulating discussions and helpful suggestions about this work.

REFERENCES

1. Steinert, M., Hentschel, U., and Hacker, J. (2002) *Legionella pneumophila*: An aquatic microbe goes astray, *FEMS Microbiol. Rev. 26*, 149−162.
2. Wintermeyer, E., Ludwig, B., Steinert, M., Schmidt, B., Fischer, G., and Hacker, J. (1995) Influence of Site-Specifically Altered Mip Proteins on Intracellular Survival of *Legionella pneumophila* in Eukaryotic Cells, *Infect. Immun. 63*, 4576−4583.
3. Kohler, R., Fanghanel, J., Konig, B., Luneberg, E., Frosch, M., Rahfeld, J. U., Hilgenfeld, R., Fischer, G., Hacker, J., and Steinert, M. (2003) Biochemical and functional analyses of the Mip protein: Influence of the N-terminal half and of peptidylprolyl isomerase activity on the virulence of *Legionella pneumophila*, *Infect. Immun. 71*, 4389−4397.
4. Wagner, C., Khan, A. S., Kamphausen, T., Schmausser, B., Lorenz, U., Fischer, G., Hacker, J., and Steinert, M. (2006) Collagen binding protein Mip enables *Legionella pneumophila* to transmigrate through the lung epithelial barrier, *Cell. Microbiol.* (in press).

5. Schmidt, B., Rahfeld, J., Schierhorn, A., Ludwig, B., Hacker, J., and Fischer, G. (1994) A Homodimer Represents an Active Species of the Peptidyl-Prolyl Cis/Trans Isomerase Fkbp25mem from *Legionella pneumophila*, *FEBS Lett. 352*, 185−190.
6. Helbig, J. H., Luck, P. C., Steinert, M., Jacobs, E., and Witt, M. (2001) Immunolocalization of the Mip protein of intracellularly and extracellularly grown Legionella pneumophila, *Lett. Appl. Microbiol. 32*, 83−88.
7. Riboldi-Tunnicliffe, A., Konig, B., Jessen, S., Weiss, M. S., Rahfeld, J., Hacker, J., Fischer, G., and Hilgenfeld, R. (2001) Crystal structure of Mip, a prolylisomerase from *Legionella pneumophila*, *Nat. Struct. Biol. 8*, 779−783.
8. Fischer, G., Bang, H., Ludwig, B., Mann, K., and Hacker, J. (1992) Mip Protein of *Legionella pneumophila* Exhibits Peptidyl-Prolyl-Cis Trans Isomerase (Pplase) Activity, *Mol. Microbiol. 6*, 1375−1383.
9. Chang, S. L., Szabo, A., and Tjandra, N. (2003) Temperature dependence of domain motions of calmodulin probed by NMR relaxation at multiple fields, *J. Am. Chem. Soc. 125*, 11379−11384.
10. Dvoretsky, A., Abusamhadneh, E. M., Howarth, J. W., and Rosevear, P. R. (2002) Solution structure of calcium-saturated cardiac troponin C bound to cardiac troponin I, *J. Biol. Chem. 277*, 38565−38570.
11. Kay, L. E., Torchia, D. A., and Bax, A. (1989) Backbone dynamics of proteins as studied by ^{15}N inverse detected heteronuclear NMR spectroscopy: Application to staphylococcal nuclease, *Biochemistry 28*, 8972−8979.
12. Fushman, D., Varadan, R., Assfalg, M., and Walker, O. (2004) Determining domain orientation in macromolecules by using spin-relaxation and residual dipolar coupling measurements, *Prog. Nucl. Magn. Reson. Spectrosc. 44*, 189−214.
13. Yoshida, T., Oka, S., Uchiyama, S., Nakano, H., Kawasaki, T., Ohkubo, T., and Kobayashi, Y. (2003) Characteristic domain motion in the ribosome recycling factor revealed by N-15 NMR relaxation experiments and molecular dynamics simulations, *Biochemistry 42*, 4101−4107.
14. Horstmann, M., Kamphausen, T., Schweimer, K., Steinert, M., Hacker, J., Haase, A., Rosch, P., Fischer, G., and Faber, C. (2005) H-1, C-13, N-15 backbone and side chain resonance assignment of Mip(77−213) the PPIase domain of the *Legionella pneumophila* Mip protein, *J. Biomol. NMR 31*, 77−78.
15. Delaglio, F., Grzesiek, S., Vuister, G. W., Zhu, G., Pfeifer, J., and Bax, A. (1995) Nmrpipe: A Multidimensional Spectral Processing System Based on Unix Pipes, *J. Biomol. NMR 6*, 277−293.
16. Pervushin, K., Riek, R., Wider, G., and Wuthrich, K. (1997) Attenuated T-2 relaxation by mutual cancellation of dipole−dipole coupling and chemical shift anisotropy indicates an avenue to NMR structures of very large biological macromolecules in solution, *Proc. Natl. Acad. Sci. U.S.A. 94*, 12366−12371.
17. Johnson, B. A., and Blevins, R. A. (1994) NMR View: A Computer-Program for the Visualization and Analysis of NMR Data, *J. Biomol. NMR 4*, 603−614.
18. Wishart, D. S., and Case, D. A. (2001) Use of chemical shifts in macromolecular structure determination, *Methods Enzymol. 338*, 3−34.
19. Wishart, D. S., Sykes, B. D., and Richards, F. M. (1992) The chemical shift index: A fast and simple method for the assignment of protein secondary structure through NMR spectroscopy, *Biochemistry 31*, 1647−1651.
20. Dayie, K. T., and Wagner, G. (1994) Relaxation-Rate Measurements for N-15-H-1 Groups with Pulsed-Field Gradients and Preservation of Coherence Pathways, *J. Magn. Reson., Ser. A 111*, 121−126.
21. Markus, M. A., Dayie, K. T., Matsudaira, P., and Wagner, G. (1994) Effect of Deuteration on the Amide Proton Relaxation Rates in Proteins: Heteronuclear NMR Experiments on Villin 14t, *J. Magn. Reson., Ser. B 105*, 192−195.
22. Tollinger, M., Skrynnikov, N. R., Mulder, F. A. A., Forman-Kay, J. D., and Kay, L. E. (2001) Slow dynamics in folded and unfolded states of an SH3 domain, *J. Am. Chem. Soc. 123*, 11341−11352.
23. Mulder, F. A. A., Skrynnikov, N. R., Hon, B., Dahlquist, F. W., and Kay, L. E. (2001) Measurement of slow (μs-ms) time scale dynamics in protein side chains by N-15 relaxation dispersion NMR spectroscopy: Application to Asn and Gln residues in a cavity mutant of T4 lysozyme, *J. Am. Chem. Soc. 123*, 967−975.
24. Blackledge, M., Cordier, F., Dosset, P., and Marion, D. (1998) Precision and uncertainty in the characterization of anisotropic rotational diffusion by N-15 relaxation, *J. Am. Chem. Soc. 120*, 4538−4539.
25. Dosset, P., Hus, J. C., Blackledge, M., and Marion, D. (2000) Efficient analysis of macromolecular rotational diffusion from heteronuclear relaxation data, *J. Biomol. NMR 16*, 23−28.
26. Berendsen, H. J. C., Vanderspoel, D., and Vandrunen, R. (1995) Gromacs: A Message-Passing Parallel Molecular-Dynamics Implementation, *Comput. Phys. Commun. 91*, 43−56.
27. Lindahl, E., Hess, B., and van der Spoel, D. (2001) GROMACS 3.0: A package for molecular simulation and trajectory analysis, *J. Mol. Model. 7*, 306−317.
28. Van der Spoel, D., Lindahl, E., Hess, B., Groenhof, G., Mark, A. E., and Berendsen, H. J. C. (2005) GROMACS: Fast, flexible, and free, *J. Comput. Chem. 26*, 1701−1718.
29. Berendsen, H. J. C., Postma, J. P. M., Van Gunsteren, W. F., and Hermans, J. (1981) *Interaction models for water in relation to protein hydration*, D. Reidel Publishing Co., Dordrecht, The Netherlands.
30. Darden, T., York, D., and Pedersen, L. (1993) Particle Mesh Ewald: An N.Log(N) Method for Ewald Sums in Large Systems, *J. Chem. Phys. 98*, 10089−10092.
31. Berendsen, H. J. C., Postma, J. P. M., Vangunsteren, W. F., Dinola, A., and Haak, J. R. (1984) Molecular-Dynamics with Coupling to an External Bath, *J. Chem. Phys. 81*, 3684−3690.
32. Hess, B., Bekker, H., Berendsen, H. J. C., and Fraaije, J. G. E. M. (1997) LINCS: A linear constraint solver for molecular simulations, *J. Comput. Chem. 18*, 1463−1472.
33. Soares, T. A., Oostenbrink, C., van Gunsteren, W. F., Daura, X., and Smith, L. J. (2004) Validation of the GROMOS force-field parameter set 45A3 against nuclear magnetic resonance data of hen egg lysozyme, *J. Biomol. NMR 30*, 407−422.
34. Amadei, A., Linssen, A. B. M., and Berendsen, H. J. C. (1993) Essential Dynamics of Proteins, *Proteins: Struct., Funct., Genet. 17*, 412−425.
35. Mu, Y. G., Nguyen, P. H., and Stock, G. (2005) Energy landscape of a small peptide revealed by dihedral angle principal component analysis, *Proteins: Struct., Funct., Bioinf. 58*, 45−52.
36. Van Aalten, D. M. F., Findlay, J. B. C., De Groot, B. L., Berendsen, H. J. C., and Amadei, A. (1997) A comparison of techniques for calculating protein essential dynamics, *J. Comput. Chem. 18*, 169−181.
37. Allen, M. P., and Tildesley, D. J. (1987) *Computer Simulations of Liquids*, Oxford Science Publications, Oxford, U.K.
38. de la Torre, J. G., Huertas, M. L., and Carrasco, B. (2000) HYDRONMR: Prediction of NMR relaxation of globular proteins from atomic-level structures and hydrodynamic calculations, *J. Magn. Reson. 147*, 138−146.
39. Tjandra, N., Kuboniwa, H., Ren, H., and Bax, A. (1995) Rotational-Dynamics of Calcium-Free Calmodulin Studied by N-15-NMR Relaxation Measurements, *Eur. J. Biochem. 230*, 1014−1024.
40. Loria, J. P., Rance, M., and Palmer, A. G. (1999) A relaxation-compensated Carr-Purcell-Meiboom-Gill sequence for characterizing chemical exchange by NMR spectroscopy, *J. Am. Chem. Soc. 121*, 2331−2332.
41. Palmer, A. G., Kroenke, C. D., and Loria, J. P. (2001) Nuclear magnetic resonance methods for quantifying microsecond-to-millisecond motions in biological macromolecules, *Methods Enzymol. 339*, 204−238.
42. Meirovitch, E., Shapiro, Y. E., Polimeno, A., and Freed, J. H. (2006) Protein dynamics from NMR: The slowly relaxing local structure analysis compared with model-free analysis, *J. Phys. Chem. A 110*, 8366−8396.
43. Prompers, J. J., and Bruschweiler, R. (2002) General framework for studying the dynamics of folded and nonfolded proteins by NMR relaxation spectroscopy and MD simulation, *J. Am. Chem. Soc. 124*, 4522−4534.
44. Idiyatullin, D., Daragan, V. A., and Mayo, K. H. (2003) (NH)-N-15 backbone dynamics of protein GB1: Comparison of order parameters and correlation times derived using various "model-free" approaches, *J. Phys. Chem. B 107*, 2602−2609.
45. Banci, L., Bertini, I., Cantini, F., Chasapis, C. T., Hadjiliadis, N., and Rosato, A. (2005) A NMR study of the interaction of a three-domain construct of ATP7A with copper(I) and copper(I)-HAH1: The interplay of domains, *J. Biol. Chem. 280*, 38259−38263.

46. Fiorin, G., Biekofsky, R. R., Pastore, A., and Carloni, P. (2005) Unwinding the helical linker of calcium-loaded calmodulin: A molecular dynamics study, *Proteins: Struct., Funct., Bioinf. 61*, 829−839.
47. Pervushin, K. V. (2005) Experimental Nuclear Magnetic Resonance Conference, Providence, RI.
48. Saul, F. A., Arie, J. P., Normand, B. V. L., Kahn, R., Betton, J. M., and Bentley, G. A. (2004) Structural and functional studies of FkpA from *Escherichia coli*, a cis/trans peptidyl-prolyl isomerase with chaperone activity, *J. Mol. Biol. 335*, 595−608.

BI060818I